

## Research Article

## Performance Analysis of a Drone Development Kit-derived Digital Elevation Model

Mehmet Doğruluk<sup>1,\*</sup>, Ilyas Yalçın<sup>2</sup><sup>1,2</sup> Department of Architecture and Urban Planning, Baskent Chamber of Industry Organized Industrial Zone Vocational School, Hacettepe University, Ankara, Türkiye

\* Corresponding author: M. Doğruluk

\* E-mail: mehmet.dogruluk@hacettepe.edu.tr

Received 17.08.2023

Accepted 02.12.2023

**How to cite:** Doğruluk, M. & Yalçın, N. (2023). Performance Analysis of a Drone Development Kit-derived Digital Elevation Model. *International Journal of Environment and Geoinformatics (IJECEO)*, 10(4): 077-089. doi. 10.30897/ijegeo.1344526

## Abstract

Surface modeling constitutes a crucial aspect in numerous engineering inquiries and earth observation endeavors. In contemporary times, the acquisition of geospatial data essential for the digital representation of local regions is increasingly facilitated through drone-based methodologies, supplanting conventional terrestrial data gathering techniques. The market presently hosts a plethora of cost-effective, "ready-to-fly" unmanned aerial vehicles (UAVs), offering users the capability to generate photogrammetric outputs, including high geometric precision Digital Elevation Models (DEMs). Moreover, modularly structured drone development kits, designed for multifarious applications, are readily accessible for purchase. These drone kits offer an economically advantageous platform that users can customize to suit their specific needs. Nevertheless, the geometric precision of DEMs created using these kits hinges upon the capabilities of the imaging and navigation systems, in addition to the stabilization of the platform during autonomous flight. In this study, using a drone development kit and a commercial drone, simultaneous image acquisition was performed for the same study area and two different DEMs were produced. The efficacy of the DEM generated using the drone development kit was assessed through a comparative analysis with the DEM obtained from a commercial drone. In addition, geometric accuracy assessment was conducted for both DEMs using ground control points. The findings demonstrated the effectiveness of drone development kits in generating DEMs with centimeter-level precision, positioning them as competitive alternatives to commercial UAVs. However, certain limitations were identified that had an adverse impact on the overall quality of the DEM generated from the drone kit. We address these challenges and offer several recommendations to overcome them.

**Keywords:** Drone development kit, Unmanned aerial vehicle, Digital elevation model, Geometric accuracy, Point cloud, Visible light camera

## Introduction

Digital elevation models (DEMs) are an important source of geospatial information for earth science and many engineering applications (Uysal et al., 2015). DEMs can be categorized into two main types: digital terrain models (DTMs) and digital surface models (DSMs). A DTM captures the elevation related to the Earth's topography, specifically excluding man-made structures and retaining only natural features. Conversely, a DSM represents the elevation of the Earth's surface, encompassing all objects present, both natural and man-made. In scientific literature, DEM is commonly employed as a generic term covering both DTM and DSM (Guth et al., 2021; Habib et al., 2017; Shawky et al., 2019).

In the last decade, different remote sensing systems such as visible light and multispectral cameras, Light Detection and Ranging (LiDAR) have been used as payloads of unmanned aerial vehicles (UAVs) or drones (Akturk and Altunel, 2019; Carpenter et al., 2023; Zhang and Zhu, 2023). Nevertheless, visible light cameras continue to maintain their prevalence and dominance among the available options for DEM production, primarily attributed to their cost-effectiveness (Bi et al., 2021; Giordan et al., 2020; Kovanič et al., 2023).

In recent years, a multitude of UAV platforms has been developed and made available for purchase, all tailored to fulfill this particular purpose. These platforms, commonly referred to as commercial UAVs, are equipped with supplementary hardware designed for accurate and real-time positioning, sophisticated camera systems, and stabilization mechanisms to ensure the stability of the UAV during operations (Kalacska et al., 2020; Bayırhan and Gazioğlu, 2020; Gündüz, 2023). Many professional users who aim to produce detailed and reliable DEMs prefer these UAVs (Deliry and Avdan, 2021; Wang and Shu, 2022). When evaluated in terms of non-professional users, the acquisition cost of commercial UAVs is still high. Currently, there are many ready-to-fly UAVs on the market that can be an alternative to commercial UAVs. These UAVs, referred to as low-cost UAVs usually have low-cost navigation systems, sensors, and cameras. However, it has been demonstrated many times that reliable DEMs can be produced with low-cost UAVs if a specific flight plan, field work with a sufficient number of ground control points (GCPs) and camera settings are applied (Gafurov, 2021; Jiménez-Jiménez et al., 2021). Modular UAV platforms can be considered as another low-cost alternative to commercial UAVs. These UAV platforms, called "drone development kit" or "Do It Yourself (DIY)", have a main platform function where preferred equipment can be integrated. In this respect,

these platforms allow a more flexible hardware configuration than ready-to-fly UAVs (Hill and Rowan, 2022). Nonetheless, as the primary aim revolves around establishing a cost-effective platform, the endeavor to generate reliable DEMs using these UAVs becomes relatively more intricate. This complexity is attributed to the constraints posed by low-cost cameras and the challenges associated with stabilizing the platform (Lee and Kim, 2022).

In fact, although most commercial UAVs are equipped with mechanical/global shutter cameras, low-cost UAVs often have rolling shutter cameras (Zhou et al., 2020). Rolling shutter sensor scans the image from the top to the bottom line by line. The movement of the UAV during image acquisition causes a short delay between the top and bottom of the generated image (Gazioğlu et al., 2017). This causes a kind of image distortion known as the rolling/jelly artifact, which negatively affects the accuracy of the DEM produced by the structure from motion (SfM) approach (Bruno and Forlani, 2023; Incekara and Seker, 2021; Kim et al., 2020). On the other hand, depending on the stabilization of the UAV platform, its speed and the exposure time of the camera during image acquisition, motion blur may occur and SfM suffers from this distortion as well (Peng et al., 2022; Sieberth et al., 2015; Teague and Chahl, 2023). The mechanical shutter can compensate for rolling artifact, but motion blur may still occur (Pichaikuppan et al., 2014; Ventura et al., 2016). Considering all the aforementioned challenges, it becomes a question to be answered whether low-cost modular UAVs can provide the expected sensitivity, especially in DEM production with high geometric accuracy. When similar studies in the literature are analyzed, it is generally seen that commercial and ready-to-fly UAVs are compared with each other or the geometrical accuracies provided by any of them in DEM production are emphasized (Elkhrachy, 2021; Granados-Bolaños et al., 2021; Kalacska et al., 2020; Kršák et al., 2016; Michez et al., 2020). There are limited number of studies addressing the examination of photogrammetric products derived from modular UAVs (Fanta-Jende et al., 2020; Guenzi et al., 2019; Jaakkola et al., 2010). For

example, Hill (2019) produced orthomosaic with better than decimeter level accuracy using a DIY-style fixed-wing drone. Moudrý et al. (2019) reported that home-assembled fixed-wing UAVs can be used successfully in steppes and deciduous forest to generate accurate point cloud. Mah and Cryderman (2015) tested the DIY-style fixed-wing drone to produce DEM for a on a stockpile. Indeed, the flight of fixed-wing UAVs is generally more stable, whereas a camera system in a multi-rotor UAV is more sensitive to engine vibrations and sudden altitude changes (Dahlin Rodin et al., 2019; Gašparović and Jurjević, 2017). Remarkably, there exists a scarcity of research that have provided comprehensive analysis regarding the DEM generation capabilities exhibited by multi-rotor drone development kits.

In this study, a multi-rotor drone development kit was assembled for autonomous flight equipped with a visible light camera. This drone kit was employed for DEM generation, and the resulting DEM was compared with GCPs and a reference DEM produced using a commercial UAV platform. We present an analysis encompassing both model and point-based evaluations of geometric accuracy. In addition to providing this evaluation, we present a workflow tailored specifically for non-professional users. Furthermore, we investigate potential causes of issues that may arise in the production of DEMs from drone kits, offering corresponding suggestions for resolution.

## Materials and Methods

### Study Site

The study area was chosen as an industrial area of approximately 0.5 km<sup>2</sup> located within the borders of Sincan District of Ankara Province. This area has a relatively flat topography with an elevation ranging from 760 m to 805 m, except for stockpiles. In addition, there are buildings, natural areas and a part of Ankara Stream within the boundaries of the study area. Although there are no large trees in the region, many small saplings have been planted in the afforestation areas along the Ankara Stream (Figure 1).

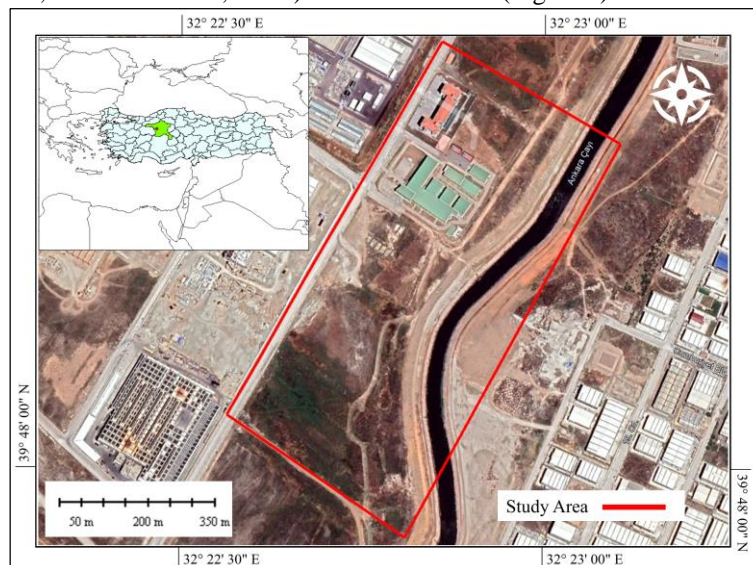


Fig. 1. Study area

## UAV Platforms

The commercial UAV platform used in this study is DJI Phantom 4 RTK. In addition to a standard GNSS (Global Navigation Satellite System) receiver, this UAV has a built-in RTK (Real Time Kinematic) module that provides centimeter-level absolute positioning accuracy to image metadata (DJI, 2023). In addition to the visible light camera, it has a 3-axis gimbal, which enables oblique view and contributes to the stabilization of the camera (Lewicka et al., 2022).

The drone kit, developed by Sapmaz Aviation and Advanced Technologies includes all the parts necessary for autonomous flight, such as battery pack, electronic speed controller, remote control, telemetry module and GNSS receiver. All parts of the drone kit have been carefully assembled and shown in Figure 2.

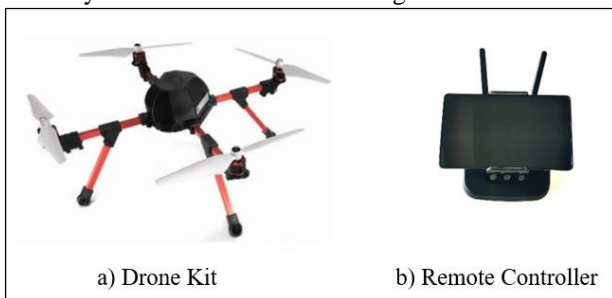


Fig.2. Assembled drone development kit. a) Drone Kit. b) Remote Controller.

After assembling the parts of the drone development kit, the camera was integrated under the kit and connected to the built-in GNSS receiver via the control card. For this purpose, a camera holder was produced from thermoplastic filament that connects the drone body and the camera. For aerial image acquisition, we used a light weight (76 g) visible light camera (MAPIR Survey 3W). This camera has a 12 megapixel (MP) Sony Exmor R IMX117 sensor (Latif, 2022). The features of the ready-to-fly drone kit are summarized in Table 1.

Table 1. Technical specifications of UAV platforms

Parts	Feature	Phantom 4 RTK	Drone Kit
Frame	Takeoff weight (g)	1391	1285
	Diagonal dist. (mm)	350	450
	Main navigation	G+GL+GA	G+GL+GA+Q
	RTK module	G+GL+GA	-
	Multi-rotor	4	4
Camera	Sensor size (")	1	1/2.3
	Focal length (mm)	8.8	3.37
	Resolution (MP)	20	12
	ISO range	100-3200	50-400
	FOV (°)	84	87
	Shutter speed (s)	1-1/2000	8-1/2000
	Shutter type	Global	Rolling
Gimbal	Stabilization	3-axis	-
	Pitch (°)	-90/+30	-
	Max controllable angular speed (°/s)	90	-
	Angular vibration range (°)	±0.02	-

\* G; GPS, GL; GLONASS, GA; GALILEO, Q; QZSS

## Flight Planning and Image Acquisition

For the Phantom 4 RTK, the DJI GS application running on the control unit with a 5.5" screen was used for flight planning. The flight planning of the drone kit was carried out using Qground Control which an open source application. For both UAVs, the front and side overlap rate of the images was chosen as 80% and 70%, respectively. Image acquisition mode was chosen as nadir and a single grid flight mission was planned instead of double-grid due to limited battery capacity in both UAV platforms. Two batteries were available for each UAVs and both were used to complete the flight missions. To keep the ground sampling distance (GSD) value close to each other, the flight altitude was set to 90 m for the Phantom 4 RTK and 60 m for the drone kit. Finally, the flight speed is set to 6 m/s for the Phantom 4 RTK and 7 m/s for the drone kit.

Simultaneous image acquisition was carried out on 20 January 2023 with both platforms. As a result of the flight, 508 and 604 images were recorded with the Phantom 4 RTK and drone kit, respectively. In the preliminary checks, we noticed that the GNSS receiver of the drone kit could not assign geotags to 18 of the images. Hence, these geotag-free images of the drone kit were excluded before image processing. The nominal GSD value of images for commercial UAV and drone kit are 0.027 m/pixel and 0.023 m/pixel, respectively. The flight plans and central projections of the acquired images are shown in Figure 3 with blue dots.

In Figure 3, the locations of geotag-free images are seen as blue dot deficiencies in the flight plan of the drone kit. Additionally, cross flight lines are also seen as both UAVs capture images while returning to the home point. In the Phantom 4 RTK, this feature is described as "Altitude Optimization" and is performed only when the mission is completed. The image is not collected when coming to home point for battery replacement. For the drone kit, this is implemented by enabling the "images in turnarounds" check box via the QGround Control software.

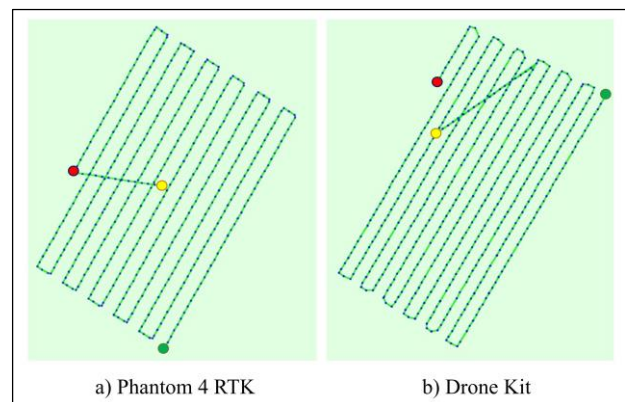


Fig. 3. Flight plans and positions of images (blue dots). Home, start and end points are shown with yellow, green and red dots, respectively. a) Phantom 4 RTK. b) Drone Kit

This configuration results in image capture not only at the end of the mission but also while returning to the home point for battery replacement. We activated this feature prior to the drone kit's flight. However, as the flight was manually terminated, images were only captured during the battery replacement phase.

### GCPs

A pivotal factor in significantly enhancing the quality of DEMs involves employing precise and evenly distributed GCPs to establish accurate connections between the model and ground truth (Villanueva and Blanco, 2019). Within the scope of the study, a total of 44 GCPs were marked, 6 of which were on the rooftops of the buildings.

GCPs are marked with red paint on the roof and blue on the concrete surfaces. On the soft surface, cube-shaped concrete blocks with a side length of 0.15 m were placed on the ground (Figure 4). The ground coordinates of the GCPs were measured with a geodetic GNSS receiver using the Network-RTK method, and 60 epoch observations were made at 1 second intervals for each point. According to the records of the GNSS receiver, the root mean square error (RMSE) values calculated for the all GCPs in the horizontal and vertical directions  $\pm 0.015$  m and  $\pm 0.019$  m, respectively. Ground coordinates of GCPs were recorded in the Turkish National Reference Frame (TUREF/TM33) projection coordinate system.

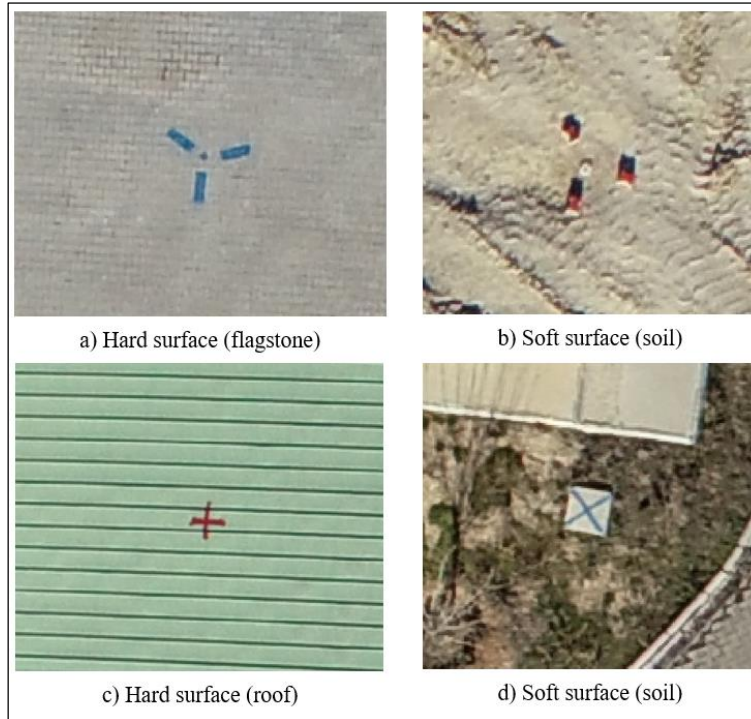


Fig. 4. Ground Markings of GCPs. a) Flagstone. b) Soil. c) Roof. d) Soil

### Image Processing

Pix4D Mapper (version 4.8.4) software was used to process the aerial images collected with both UAV platforms. After the images are added to the project, the input coordinate system is set to WGS84 (World Geodetic System 1984) as the drone data is geotagged using the onboard GNSS receiver. At this stage, the calibration parameters of the cameras used were automatically read by the software. Note that the initial calibration parameters of both cameras are available in the Pix4D's database and the rolling shutter correction option is enabled for the MAPIR 3W camera. After this process, the output coordinate system (TUREF/TM33) is set as the GCPs are recorded in this coordinate system. Image processing in Pix4D begins by extracting candidate feature points (key points) from overlapping images, and then orientation of multi-view stereo images is performed using matching feature points (tie points). At this stage, a database (sparse point cloud) is created for tie points (Pricope et al., 2019). The sparse point cloud is utilized to identify image pairs with a satisfactory number of common valid tie points, indicating the degree of their overlap. This process holds significance as it involves

generating depth maps for overlapping pairs, ultimately leading to the creation of a dense point cloud. After GCPs are added to the block and marked, some of them are assigned as GCP and bundle block adjustment is applied to optimize the camera model and reduce systematic errors in the image block. At this stage, georeferencing the sparse point cloud to a specific coordinate system is performed (Ruzgienė et al., 2015). When the SfM workflow is completed, the RMSE values of residuals at check points (CPs) are calculated. Should the resultant statistical measures prove to be satisfactory, a subsequent procedure involving point cloud expansion and filtering is executed upon the initially sparse point cloud. Following this, the generation of a dense point cloud, DEM and orthomosaic ensues, all accomplished at a predetermined resolution.

### Quality Analysis

Quality evaluation were also carried out regarding the visual evaluations of the image matching results and DEMs, as well as the RMSE values calculated for CPs as a result of the bundle block adjustment. RMSE is important in accuracy assessment of geospatial data as it serves as a measure of the magnitude of error

encompassing bias in the x, y, and z directions. The following equation was used for the sum of the RMSE errors at the CPs;

$$\text{RMSE}_T = \sqrt{\text{RMSE}_x^2 + \text{RMSE}_y^2 + \text{RMSE}_z^2} \quad (\text{Eq.1})$$

Where:  $\text{RMSE}_T$  represents the total root mean square error, and the others represent the RMSE values of the residuals in the x, y, and z directions, respectively. On the other hand, point clouds and DEMs were compared with each other to measure geometric accuracy. This approach has been used in many earth science studies and has proven to be a more effective method for determining the locality of deviations (Bailey et al., 2022; Mancini et al., 2013). Cloud to cloud comparisons were performed by applying the workflow in CloudCompare software. In this comparison, the point clouds are aligned with each other by iterative closest point (ICP) algorithm. For every point in the source point cloud, ICP identifies the closest point in the target point cloud, establishing a one-to-one correspondence between the datasets. Throughout this process, the registration error, characterized by Euclidean distances between corresponding points, is iteratively minimized (Xu et al., 2023). Afterward the mean distances between the two data sets and the standard deviation of this distance are calculated. The mean distance represents accuracy, while the standard deviation represents precision (Zapico et al., 2021). In the concept

of comparing DEMs, the spatial distribution of vertical discrepancies is tried to be revealed. The critical step in this approach is to align the compared DEMs to the same horizontal plane (Wang and Ye, 2021).

## Results

In this study, aerial image datasets were processed independently using the default settings of Pix4D software. There were two main reasons for using default parameters. Firstly, since potential users of drone kits were non-professionals, the aim was to establish a relatively simple workflow tailored to their needs. The other was to exclude the effect of the software's parameter optimization on the results from the scope of the study. Consequently, dense point clouds and DEMs were produced for both UAVs. Image processing was performed on a computer with a 3.3 GHz Intel Xeon-E2124 CPU and 5 GB Nvidia Quadro P2000 graphics card and 80 GB of system memory (RAM).

During the initial phase, the extraction of tie points was achieved through the process of image matching. The results of the matchings are visually depicted in Figure 5. Within Figure 5, areas denoted by black hues signify regions characterized by a high degree of matching success, whereas regions depicted in white hues indicate instances of inadequate image matching.

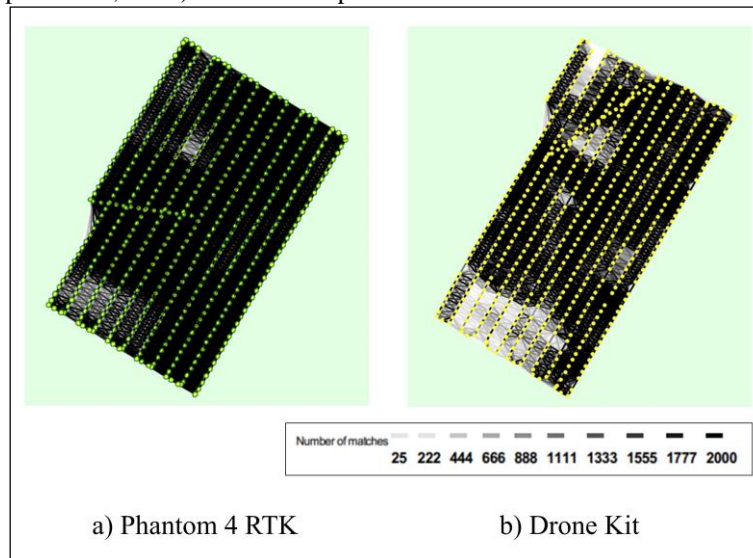


Fig. 5. Image matching maps. a) Phantom 4 RTK. b) Drone Kit

Upon scrutinizing Figure 5, it becomes apparent that the Phantom 4 RTK yields a relatively more uniform image matching map. In contrast, the matching performance of the drone kit demonstrates a discernible reduction, primarily noticeable in the northern building rooftops and southern vegetation clusters. According to Pix4D's quality report, the average number of tie points per image was calculated as 32,894 for the Phantom 4 RTK, while this value was 28,503 for the drone kit. Despite the close similarity in the average number of tie points for both UAVs, it is crucial to note a significant reduction in the minimum number of tie points calculated per image for the drone kit. Specifically, this value was calculated as

14,835 for the Phantom 4 RTK, while it was 2,651 for the drone kit. The regions depicted in white hues on the drone kit's matching map represent the corresponding location of these images. The decline in matching performance can be attributed to various factors, including repetitive texture, image scale changes, camera settings, and motion blur resulting from platform vibration (Sieberth et al., 2014). In our case, while motion blur is observable in certain drone kit images, pinpointing the exact cause of motion blur is often challenging. Detailed investigations are necessary to establish a direct link between motion blur and the stabilization of the UAV platform (Dahlin Rodin et al., 2019).

Following the completion of the image matching stage, 44 GCPs were added to the project and image coordinates were marked on at least three images for each GCP. 12 of them with homogeneous distributed in the study area were assigned as GCPs and used to self-calibration (camera model optimization) and georeferencing. The spatial distribution of GCPs in the study area corresponds to approximately 4 GCPs/ha. The remaining were assigned as CPs and used to evaluate the geometric accuracy of the

generated DEMs. The spatial distribution of GCPs and CPs is shown in Figure 6 with sparse point clouds. In the next stage, the image blocks were optimized with 12 GCPs. In this way, the scale and absolute position of the image blocks were determined. At this stage, georeferencing results were also produced by disabling Pix4D's rolling shutter (RS) correction. Statistics of residuals calculated for CPs as a result of bundle block adjustment are shown in Table 2.

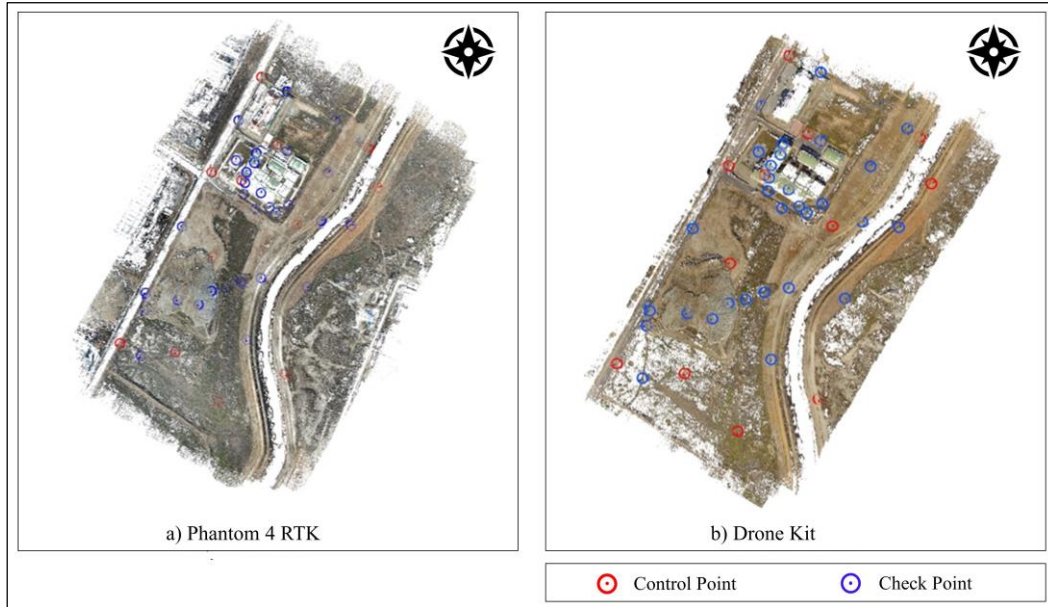


Fig. 6. Spatial distribution of GCPs and CPs in the study area.

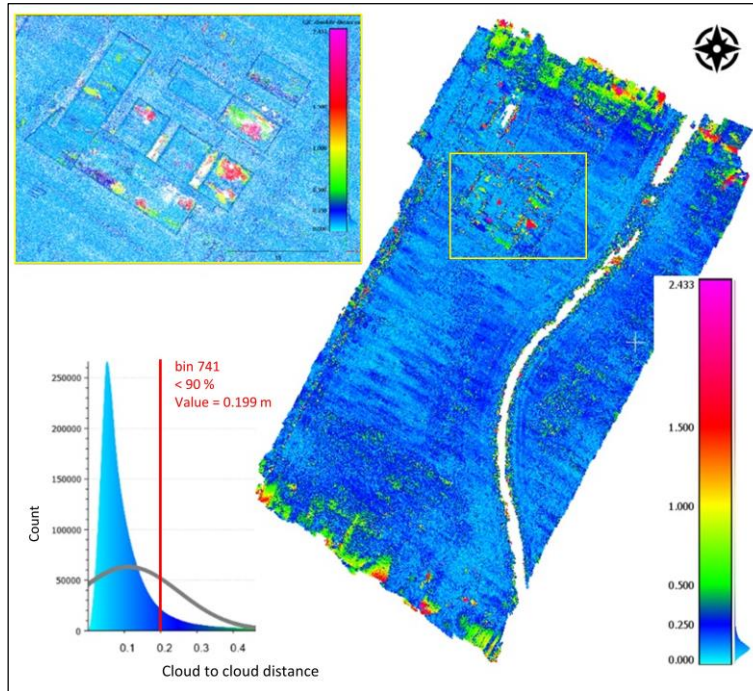


Fig. 7. Absolute distances between point clouds and their histogram. “bin 741” represents the bin number corresponding to 90% of the absolute distances in the histogram.

Table 2. RMSE values calculated for 32 CPs

UAV	RS		RMSE (m)			Total
	Correction		X	Y	Z	
P4 RTK	enable		0.014	0.018	0.030	0.038
	disable		0.015	0.017	0.030	0.038
Drone Kit	enable		0.069	0.045	0.060	0.102
	disable		0.179	0.130	0.082	0.236

When Table 2 is examined, it is clearly seen that the RS correction has a positive effect on the georeferencing results of the drone kit and the RMSE values are reduced. However, the RS correction slightly changed the Phantom 4 RTK's georeferencing results. A dense point cloud was generated for the drone kit subsequent to the application of RS correction procedures, whereas the point cloud was generated without RS correction for the Phantom 4 RTK. The density of the point cloud produced with the Phantom 4 RTK was 246 points/m<sup>2</sup>, while the point density of the drone kit was 304 points/m<sup>2</sup>.

Utilizing the aforementioned point clouds, a cloud to cloud comparison was conducted. Registration of the point clouds was achieved by using 50,000 randomly selected points, subsequently the absolute mean distances of these point clouds were calculated. The outcome of this analysis is depicted in Figure 7.

The cloud to cloud comparison yielded an absolute mean distance of 0.094 m, accompanied by a standard deviation of  $\pm 0.133$  m. These distances are visually represented in Figure 7, employing distinct colors to reflect varying magnitudes. An observation of Figure 7 reveals a

predominant concentration of absolute distances within the blue spectrum (ranging from 0 to 0.25 m). Furthermore, approximately 90% of absolute distances fall below  $\pm 0.199$  m. However, discernible elevations in mean distances are noticeable along building rooftops and the periphery of the image blocks.

Subsequent to the cloud to cloud comparison, two distinct DEMs were generated at a resolution of 0.10 m per pixel. DEM produced by Phantom 4 RTK is abbreviated as "DEM<sub>P</sub>" and the other is abbreviated as "DEM<sub>K</sub>". To clearly demonstrate the spatial distribution of vertical errors ( $\Delta z$ ) in the DEM<sub>K</sub>, cell-by-cell error raster were generated by subtracting the value in DEM<sub>K</sub> from the corresponding value of the reference model (DEM<sub>P</sub>). In this comparison, a 20 m buffer was applied to narrow down the study area, aiming to eliminate errors in the analysis that might arise from inadequate overlap in the boundary lines of the flights. The resulting raster map and the statistics of the  $\Delta z$  values are shown in Figure 8. Note that only errors in the range of  $\pm 1$  m are visualized to examine the  $\Delta z$  values in more detail, while statistics are generated based on all data.

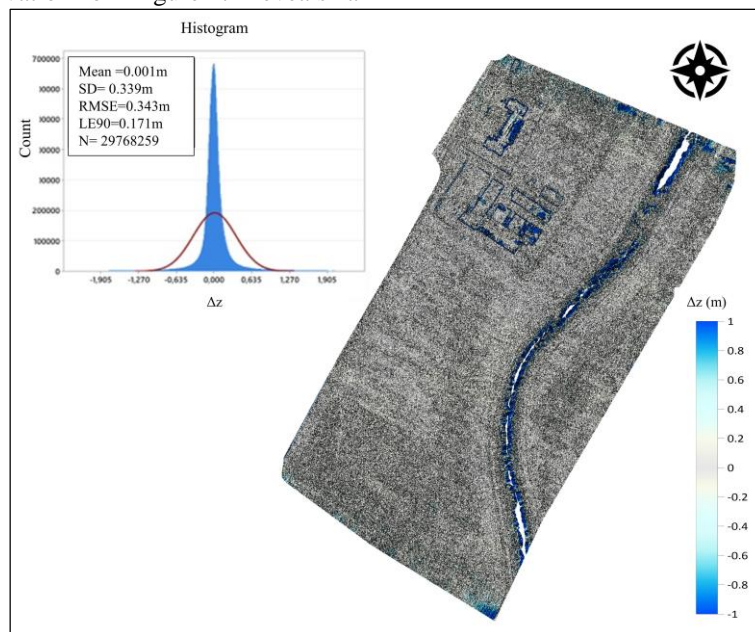


Fig. 8. Height difference map.

When Figure 8 examined, an observable trend emerges where deviations accentuate in proximity to water surfaces and surrounding buildings. Upon statistical evaluation, the RMSE values for  $\Delta z$  ( $\pm 0.343$  m) exhibit an increase when contrasted with the outcomes of the initial cloud to cloud comparison. This escalation can be attributed to inherent estimation errors arising from interpolation processes. On the other hand, it has been ascertained that 90% of linear errors (LE90) within the DEM<sub>K</sub> are contained within the range of  $\pm 0.171$  m. This finding demonstrates a slight improvement compared to the results of the cloud-to-cloud comparison, as errors occurring at the boundaries were excluded from the analysis. In summary, we demonstrate that in the presence of homogeneously distributed precise GCPs, DEMs with

centimeter-level accuracy can be generated using drone kits. In our specific case, 90% of the linear errors in this DEM were smaller than  $\pm 0.20$  m. Excluding areas where adequate overlap was not achieved resulted in a slight decrease in this value, concurrently leading to an overall increase in accuracy.

## Discussion

Within the scope of this study, the potential to generate DEMs characterized by centimeter-level geometric accuracy utilizing multi-rotor drone kits, contingent upon meticulous GCPs strategizing was demonstrated. Considering the quantitative assessment performed with CPs, an accuracy equating to a RMSE<sub>T</sub> of 0.102 m is

achieved. In contrast, the corresponding value for the commercial UAV stands at 0.038 m (as depicted in Table 2). The  $RMSE_T$  reflects the disparity between the initial and computed positions of CPs, serving as an estimation for the overall absolute accuracy of the DEM. While the application of RS correction does enhance the outcomes for the drone kit, it becomes imperative to delve further into the scrutiny of the errors occurring within the CPs. For this purpose, correlations of the computed residuals encompassing all three axes (x, y, and z) were scrutinized across the set of 32 CPs for both platforms (Table 3).

Table 3. Correlation matrix of residuals

	$x_k$	$y_k$	$z_k$	$x_p$	$y_p$	$z_p$
$x_k$	1					
$y_k$	0.17	1				
$z_k$	-0.41	-0.29	1			
$x_p$	0.06	-0.10	-0.05	1		
$y_p$	0.00	0.42	-0.06	-0.21	1	
$z_p$	0.22	0.23	0.12	-0.34	0.21	1

According to the Table 3, it was deduced that there existed no noteworthy correlation among the residuals. This observation underscored the absence of a substantial connection between the residuals and the positional errors inherent to the CPs themselves. This indicates that the generated DEMs do not exhibit a significant bias with each other. Afterward, boxplot charts were generated to visually represent the statistical distribution of residuals for the CPs (Figure 9). The central horizontal lines in the boxes represent median values and the symbol x represents mean values in Figure 9.

Considering the box lengths, it is clear that the variation of the residuals increases in all directions ( $x_k$ ,  $y_k$  and  $z_k$ ) for the drone kit. In addition, the residual ranges are higher than the Phantom 4 RTK. Given that both sets of images were processed with the same software, the observed increase in error magnitudes in the residuals can be attributed to the drone kit's GNSS receiver, lower specification camera, and the absence of a camera stabilization system.

On the other hand, in model-based evaluations, it is seen that 90% of the errors are concentrated in a range of about 0.20 m, which is consistent with the point-based evaluation results. However, it was observed that the magnitude of the errors increased dramatically some characteristic regions of the study area. On bare ground, planted areas and stockpile the errors varied within a small range but increased especially on the rooftops of the buildings. The comparative manifestation of these errors and data gaps within the  $DEM_k$  is strikingly illustrated in Figure 10.

In Figure 10-a, data gaps and noises on the rooftops are clearly seen. These variations negatively affect the results of the point and model-based comparisons performed in this study and reduce the overall reliability and quality (e.g. completeness) of the DEM obtained from the drone kits. Moreover, in applications such as change detection, this could lead to the non-detection of changes or their misinterpretation as false positives. Indeed, at low flight altitudes, image matching difficulties arise when reconstructing rooftops, even if 80% overlap is used. These difficulties arise from both sudden image scale changes due to building heights and repetitive textures in images (Hong-Xia et al., 2013; Santise et al., 2014). Unlike rooftops, the absence of significant noise and data gaps in areas with poor image matching at ground level (Figure 10-c, e, g) indicates that the problem is caused by sudden image scale changes. However, it should not be overlooked that the micro-level details are less represented in the  $DEM_k$  (Figure 10-g). Nonetheless, if the already poorly represented micro-level details is deemed negligible, subsequent to the cleaning of noisy points within the point cloud utilizing a suitable filtering methodology (e.g. statistical outlier removal), the generation of a DEM employing a pertinent interpolation technique (e.g. inverse distance weighting or kriging) could potentially augment the precision of outcomes. However, diminishing the details may impose limitations on the applications of the DEM derived from the drone kit. Notably, the level of detail (LoD) plays a crucial role in the creation of 3D city models. Reducing micro details can result in the regression of the produced model to a lower level (e.g. LoD2 instead of LoD3) impacting its accuracy (Ergun et al., 2023).

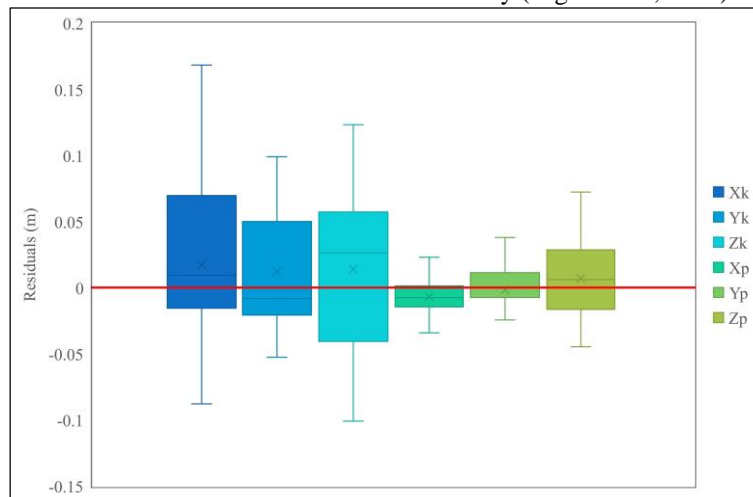


Fig. 9. Boxplot graph of residuals. Blue tones represent the drone kit, green tones represent the Phantom 4 RTK.

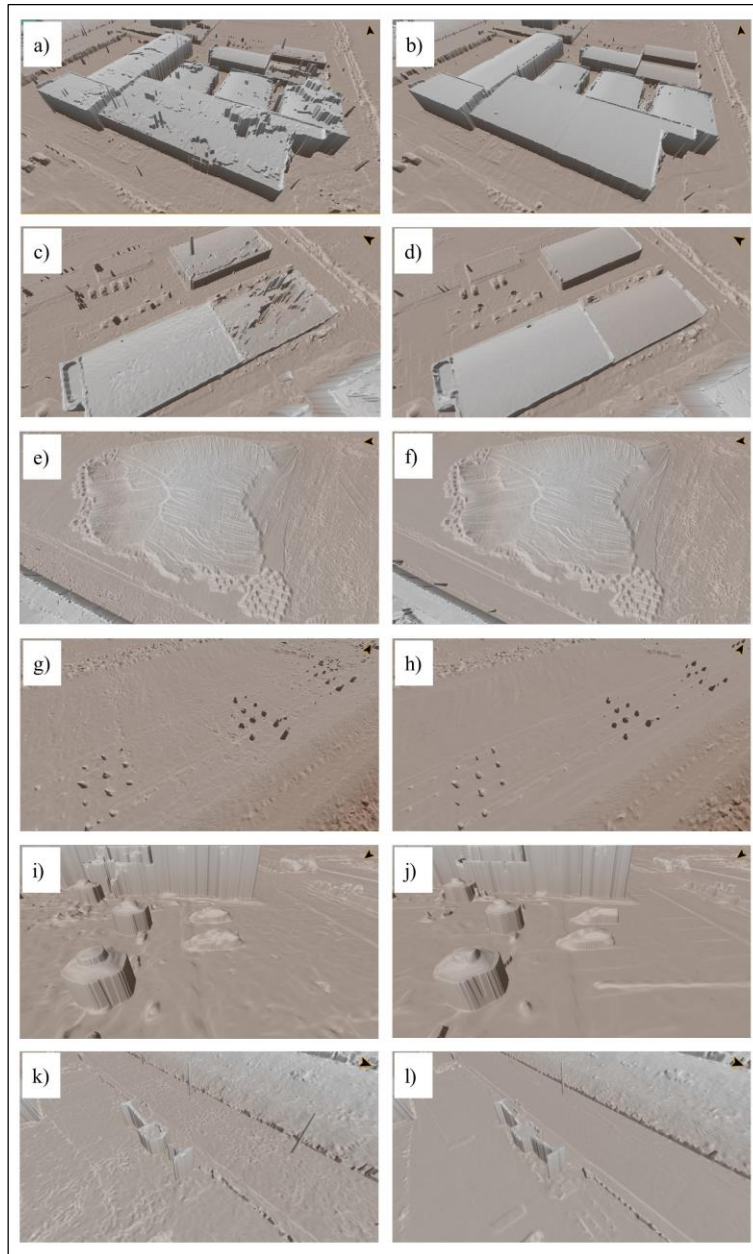


Fig. 10. Perspective views of DEMs. a), c), e), g), i), k) represent  $DEM_K$ . b), d), f), h), j), l) represent  $DEM_P$ .

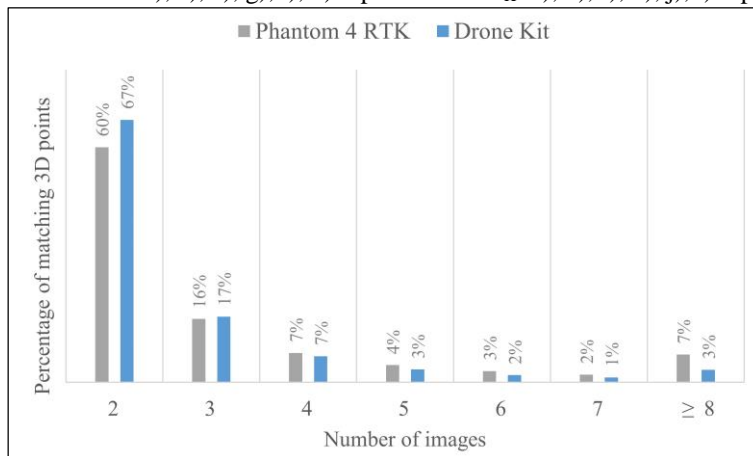


Fig. 11. Percentage of 3D points observed from UAVs images.

Certainly, regardless of the underlying reasons, difficulties in image matching have a direct impact on the triangulation phase, where camera parameters are employed to create a point cloud from the tie points.

Considering that each 3D point is generated from tie points observed in at least two images, it can be deduced that 3D points derived from a smaller number of images (e.g. 3 images) are less reliable than those derived from a

larger number of images (e.g. 5 images) (Rhee and Kim, 2016). In our case, we analyzed sparse point clouds and generated a graph to enhance our understanding of the number of images from which the generated 3D points originated (Figure 11).

Upon examination of Figure 11, for both UAVs, it is evident that the majority of the 3D points constituting the sparse point cloud are derived from 2, 3 or 4 images. However, a consistent rise is observed with the Phantom 4 RTK, particularly beyond 4 images, and the percentage of points generated from  $\geq 8$  images is more than double that of the drone kit. Although this may not appear to represent a substantial quantity of 3D points, it actually corresponds to approximately 360,000 and 190,000 points for the Phantom 4 RTK and drone kit, respectively, even within the sparse point cloud. Consequently, it is unsurprising that the Phantom 4 RTK exhibits fewer noisy points and produces a more reliable point cloud compared to the drone kit.

Another well-known factor that influences the quality of the resulting products of UAVs is motion blur. In our case, a notable presence of motion blur was evident in some images acquired using the drone kit, in contrast to the imagery obtained through the Phantom 4 RTK. Considering that the meteorological conditions during image acquisition for both UAVs are similar, the reason for motion blur can be related to the flight speed, stabilization and camera settings of the drone kit. The exposure of a frame camera is regulated by parameters such as shutter speed, aperture (f-number) and ISO value, regardless of the flight speed of the platform. However, Roth et al. (2018) proposed the following equation, which considers flight speed ( $v$ ), GSD value, and shutter speed ( $t$ ) to calculate theoretical motion blur ( $b$ ) caused by the forward motion of the platform.

$$b = \frac{v \cdot t}{\text{GSD}} \quad (\text{Eq.2})$$

They suggested that the shutter speed should be fast enough to prevent motion blur and keeping motion blur smaller than  $0.5 \cdot \text{GSD}$  for each image. According to this approach, the shutter speeds of the drone kit and Phantom 4 RTK were supposed to be faster than  $1/600$  s and  $1/444$  s respectively. For the Phantom 4 RTK with a built-in gimbal, shutter speed, aperture and ISO are automatically adjusted according to flight speed and sensor sensitivity, keeping the expected image motion blur at the sensor pixel size (Sertić et al., 2022). Therefore, the shutter speed limit value may have been kept more flexible for the Phantom 4 RTK during the flight mission. During the flight of the drone kit, the camera parameters were configured in automatic mode, thereby attaining a harmonious equilibrium among factors such as ISO, aperture and shutter speed. Nevertheless, the drone kit lacked a functional mechanism capable of establishing a congruence between the camera system and the stabilization of the aerial platform during the flight operations. Hence, our attention was directed towards investigating the possible occurrence of motion blur in images surpassing the computed theoretical threshold for

shutter speed. The specific shutter speeds associated with each image in the drone kit were extracted using ExifTool (Harvey and Körtner, 2016). Additionally, despite the flight being conducted with the cameras in auto mode, the camera settings and configurations utilized for both the drone kit and the Phantom 4 RTK are outlined in Table 4. The shutter speeds of the drone kit images are in the range of  $1/227$ - $1/885$  s. However, in the examinations conducted on images captured using low shutter speeds, a substantial correlation between motion blur and shutter speed was not identified.

Table 4. The camera settings of UAVs

	Phantom 4 RTK	Drone kit
Shutter Speed (1/s)	1/200-1/500	1/227-1/885
Range		
Aperture (f-Number)	f/5.6	f/2.8
ISO	100	50

Despite all these efforts, there was difficulty in determining the exact cause of the motion blur and whether it could be directly linked to the stabilization of the drone kit. To address this issue, we ascribe the undertaking of a more extensive examination into the impacts of parameters, such as flight speed and shutter speed, on image quality and motion blur, to forthcoming endeavors utilizing two distinct visible light cameras mounted on a drone kit. Hence, we anticipate that by employing two cameras with different settings on a single drone kit, we can investigate whether motion blur is directly linked to the stabilization of the drone kit. Based on current results, we recommend choosing slower (e.g. 6 m/s) flight speeds and higher shutter speeds (e.g.  $1/750$  s) to set before flight to avoid motion blur when acquiring images with drone development kits.

## Conclusion

The performance of geospatial data collection of UAV platforms has been a hot topic of interest for researchers for a long time. Nowadays, commercial UAVs outfitted with cutting-edge instrumentation effortlessly and accurately execute this undertaking. Nevertheless, the relatively high cost associated with commercial UAV platforms compels non-professional users to explore alternative solutions. The increasing interest in low-cost UAVs in geospatial data collection can be evaluated as a result of these trends. Today, access to low-cost UAVs, for example, weighing less than 250 grams and equipped with a three-axis gimbal (e.g. DJI Mini 4 Pro), has become easier than ever and is accessible for around \$760. On the other hand, the Phantom 4 RTK, considered one of the more affordable commercial UAVs in its class, is available for approximately \$6,600. However, users who will prefer such low-cost UAVs need concrete information for cost-benefit optimization. Although there is a considerable amount of research on the creation of photogrammetric products such as DEMs using ready-to-fly UAVs, research on modular UAV platforms that can be procured in a fully modular structure and made ready-to-fly by users is limited. The dominance of ready-to-fly

UAVs in the market and their relative ease of use may be the reason for this limitation. But when it comes to collecting geospatial data or generating DEMs, the quality of the end products is often directly related to equipment selection and their fine-tuning. Ready-to-fly UAVs substantially restrict the extent to which users can select equipment and manipulate its parameters.

Modular UAVs exhibit advantages of cost-effectiveness and enablement of heightened flexibility in terms of payload arrangement and meticulous adjustments, in contrast to their ready-to-fly counterparts. Moreover, different remote sensing sensors can be integrated on these platforms at the same time and are less affected by wind due to their reasonable weight. For instance, both a visible light and a multispectral camera can be concurrently integrated into the modular UAV. This enables the acquisition of not only geometric information but also richer spectral information for the area of interest. Undoubtedly, alongside this flexibility, there exist challenges, notably the imperative to acquire GCPs compared to commercial UAVs. Although field works are the most time-consuming process of geospatial data generation using UAVs, GCPs are still needed to eliminate distortions (e.g. doming effect) in the end products, even when using commercial UAVs. It is emphasized that even the inclusion of just 1 GCP significantly reduces vertical bias, and having at least 1 GCP per 100 images enhances the overall accuracy of the resulting products. From this point of view, low-cost modular UAVs can be preferred, probably considering the field work involving a higher number of GCPs than commercial UAVs. Although marking GCPs on the ground typically does not significantly inflate costs, the heightened workload and prolonged duration of field work may contribute to an increase in the overall cost. Considering that the cost of the commercial UAV platform employed in this study is roughly four times higher than that of the modular UAV (approximately \$1000 including all components), it is evident that modular UAVs with a comparable flight mission duration (about 30 minutes) will remain an appealing alternative.

### Acknowledgements

This study was supported by Hacettepe University Scientific Research Project Coordination Unit within the scope of the project numbered FAY-2022-19793. We thank Hacettepe University for providing this support. We also thank Abdurrahman Gürel for his contributions in making the drone development kit ready for autonomous flight.

### References

- Akturk, E., Altunel, A. O. (2019). Accuracy Assessment of a Low-Cost UAV Derived Digital Elevation Model (DEM) in a Highly Broken and Vegetated Terrain. *Measurement*, 136, 382-386. <https://doi.org/https://doi.org/10.1016/j.measurement.2018.12.101>
- Bailey, G., Li, Y., McKinney, N., Yoder, D., Wright, W., Washington-Allen, R. (2022). Las2DoD: Change Detection Based on Digital Elevation Models Derived from Dense Point Clouds with Spatially Varied Uncertainty. *Remote Sensing*, 14(7), 1537. <https://www.mdpi.com/2072-4292/14/7/1537>
- Bayırhan, I., Gazioğlu, C. (2020). Use of Unmanned Aerial Vehicles (UAV) and Marine Environment Simulator in Oil Pollution Investigations, *Baltic J. Modern Computing*, 8(2), 327-336, doi.10.22364/bjmc.2020.8.2.08
- Bi, R., Gan, S., Yuan, X., Li, R., Gao, S., Luo, W., Hu, L. (2021). Studies on Three-Dimensional (3D) Accuracy Optimization and Repeatability of UAV in Complex Pit-Rim Landforms As Assisted by Oblique Imaging and RTK Positioning. *Sensors*, 21(23), 8109.
- Bruno, N., Forlani, G. (2023). Experimental Tests and Simulations on Correction Models for the Rolling Shutter Effect in UAV Photogrammetry. *Remote Sensing*, 15(9), 2391.
- Carpenter, A., Lawrence, J. A., Ghail, R., Mason, P. J. (2023). The Development of Copper Clad Laminate Horn Antennas for Drone Interferometric Synthetic Aperture Radar. *Drones*, 7(3), 215.
- Dahlin Rodin, C., de Alcantara Andrade, F. A., Hovenburg, A. R., Johansen, T. A. (2019). A Survey of Practical Design Considerations of Optical Imaging Stabilization Systems for Small Unmanned Aerial Systems. *Sensors*, 19(21), 4800.
- Deliry, S. I., Avdan, U. (2021). Accuracy of Unmanned Aerial Systems Photogrammetry and Structure from Motion in Surveying and Mapping: A Review. *Journal of the Indian Society of Remote Sensing*, 49(8), 1997-2017. <https://doi.org/10.1007/s12524-021-01366-x>
- DJI. (2023). *DJI Enterprise Phantom 4 RTK Specifications*. Retrieved 26 July 2023 from <https://enterprise.dji.com/phantom-4-rtk/specs>
- Elkhrachy, I. (2021). Accuracy Assessment of Low-Cost Unmanned Aerial Vehicle (UAV) Photogrammetry. *Alexandria Engineering Journal*, 60(6), 5579-5590. <https://doi.org/https://doi.org/10.1016/j.aej.2021.04.011>
- Ergun, B., Sahin, C., Bilucan, F. (2023). Level of Detail (LoD) Geometric Analysis of Relief Mapping Employing 3D Modeling via UAV Images in Cultural Heritage Studies. *Heritage Science*, 11(1), 194. <https://doi.org/10.1186/s40494-023-01041-z>
- Fanta-Jende, P., Steininger, D., Bruckmüller, F., Sulzbachner, C. (2020). A Versatile UAV Near Real-Time Mapping Solution for Disaster Responses – Concept, Ideas and Implementation. *Int. Arch. Photogramm. Remote Sens. Spatial Inf. Sci.*, XLIII-B1-2020, 429-435. <https://doi.org/10.5194/isprs-archives-XLIII-B1-2020-429-2020>
- Gazioğlu, C., Varol, ÖE., Şeker, DZ., Çağlar, N. (2017). Determination of the Environmental Impacts of Marine Accidents Using UAV and RS Technologies, *19th MESAEP Symposium on Environmental and Health Inequity*, Roma, ITALYA, 3-6 Dec 2017.
- Gafurov, A. (2021). The Methodological Aspects of Constructing a High-Resolution DEM of Large Territories Using Low-Cost UAVs on the Example of the Sarycum Aeolian Complex, Dagestan, Russia. *Drones*, 5(1), 7.

- Gašparović, M., Jurjević, L. (2017). Gimbal Influence on the Stability of Exterior Orientation Parameters of UAV Acquired Images. *Sensors*, 17(2), 401.
- Giordan, D., Adams, M. S., Aicardi, I., Alicandro, M., Allasia, P., Baldo, M., De Berardinis, P., Dominici, D., Godone, D., Hobbs, P., Lechner, V., Niedzielski, T., Piras, M., Rotilio, M., Salvini, R., Segor, V., Sotier, B., Troilo, F. (2020). The Use of Unmanned Aerial Vehicles (UAVs) for Engineering Geology Applications. *Bulletin of Engineering Geology and the Environment*, 79(7), 3437-3481. <https://doi.org/10.1007/s10064-020-01766-2>
- Granados-Bolaños, S., Quesada-Román, A., Alvarado, G. E. (2021). Low-Cost UAV Applications in Dynamic Tropical Volcanic Landforms. *Journal of Volcanology and Geothermal Research*, 410, 107143. <https://doi.org/https://doi.org/10.1016/j.jvolgeores.2020.107143>
- Guenzi, D., Allasia, P., Baldo, M., Giordan, D. (2019). Open Source, Low-Cost and Modular Fixed-Wing UAV with BVLOS Flight Capabilities for Geohazards Monitoring and Surveying. 2019 IEEE 5th International Workshop on Metrology for AeroSpace Turin, Italy.
- Guth, P. L., Van Niekerk, A., Grohmann, C. H., Muller, J.-P., Hawker, L., Florinsky, I. V., Gesch, D., Reuter, H. I., Herrera-Cruz, V., Riazanoff, S., López-Vázquez, C., Carabjal, C. C., Albinet, C., Strobl, P. (2021). Digital Elevation Models: Terminology and Definitions. *Remote Sensing*, 13(18), 3581.
- Gündüz, S. (2023). UAV Image-Based Plan Drawing Method in Submerged Terrestrial Archaeological Settlements: The case of Kibotos. *International Journal of Environment and Geoinformatics*, 10(1), 139-145. <https://doi.org/10.30897/ijegeo.1231224>
- Habib, A., Akdim, N., El Ghandour, F.-e., Labbassi, K., Khoshelham, K., Menenti, M. (2017). Extraction and accuracy assessment of high-resolution DEM and derived orthoimages from ALOS-PRISM data over Sahel-Doukkala (Morocco). *Earth Science Informatics*, 10(2), 197-217. <https://doi.org/10.1007/s12145-017-0287-5>
- Harvey, P., Körtner, G. (2016). *ExifTool*. Retrieved 12.08.2023 from <https://exiftool.org/>
- Hill, A. C. (2019). Economical Drone Mapping for Archaeology: Comparisons of Efficiency and Accuracy. *Journal of Archaeological Science: Reports*, 24, 80-91. <https://doi.org/https://doi.org/10.1016/j.jasrep.2018.12.011>
- Hill, A. C., Rowan, Y. M. (2022). The Black Desert Drone Survey: New Perspectives on an Ancient Landscape. *Remote Sensing*, 14(3), 702.
- Hong-Xia, C., De-Zhu, G., Zhuo, L. (2013). Research on Image Motion Blur for Low Altitude Remote Sensing. *Information Technology Journal*, 12(23), 7096.
- Incekara, A. H., Seker, D. Z. (2021). Rolling Shutter Effect on The Accuracy of Photogrammetric Product Produced by Low-Cost UAV. *International Journal of Environment and Geoinformatics*, 8(4), 549-553.
- Jaakkola, A., Hyypä, J., Kukko, A., Yu, X., Kaartinen, H., Lehtomäki, M., Lin, Y. (2010). A Low-Cost Multi-Sensoral Mobile Mapping System and Its Feasibility for Tree Measurements. *ISPRS Journal of Photogrammetry and Remote Sensing*, 65(6), 514-522. <https://doi.org/10.1016/j.isprsjprs.2010.08.002>
- Jiménez-Jiménez, S. I., Ojeda-Bustamante, W., Marcial-Pablo, M. d. J., Enciso, J. (2021). Digital Terrain Models Generated with Low-Cost UAV Photogrammetry: Methodology and Accuracy. *ISPRS International Journal of Geo-Information*, 10(5), 285. <https://www.mdpi.com/2220-9964/10/5/285>
- Kalacska, M., Lucanus, O., Arroyo-Mora, J. P., Laliberté, É., Elmer, K., Leblanc, G., Groves, A. (2020). Accuracy of 3D Landscape Reconstruction without Ground Control Points Using Different UAS Platforms. *Drones*, 4(2), 13.
- Kim, N., Bae, J., Kim, C., Park, S., Sohn, H.-G. (2020). Object Distance Estimation Using a Single Image Taken from a Moving Rolling Shutter Camera. *Sensors*, 20(14), 3860.
- Kovanič, L., Topitzer, B., Peřovský, P., Blišťan, P., Gergeľová, M. B., Blišťanová, M. (2023). Review of Photogrammetric and Lidar Applications of UAV. *Applied Sciences*, 13(11), 6732.
- Kršák, B., Blišťan, P., Pauliková, A., Puškárová, P., Kovanič, L., Palková, J., Zelížňaková, V. (2016). Use of Low-Cost UAV Photogrammetry to Analyze the Accuracy of A Digital Elevation Model in a Case Study. *Measurement*, 91, 276-287. <https://doi.org/10.1016/j.measurement.2016.05.028>
- Latif, M. A. (2022). Improving Stability of Aerial Videos Acquired Through Vision Sensors Onboard UAVs for Applications in Precision Agriculture. *Signal, Image and Video Processing*, 16(5), 1263-1270. <https://doi.org/10.1007/s11760-021-02077-z>
- Lee, H., Kim, D. j. (2022). Generation of Dense and High-Precision Digital Elevation Model Using Low-Cost Unmanned Aerial Vehicle and Space-Borne TanDEM-X to Measure Exposed Area Change Due to Tidal Invasion. *IEEE Journal of Selected Topics in Applied Earth Observations and Remote Sensing*, 15, 6899-6911. <https://doi.org/10.1109/JSTARS.2022.3195744>
- Lewicka, O., Specht, M., Specht, C. (2022). Assessment of the Steering Precision of a UAV along the Flight Profiles Using a GNSS RTK Receiver. *Remote Sensing*, 14(23), 6127.
- Mah, S. B., Cryderman, C. S. (2015). Implementation of An Unmanned Aerial Vehicle System for Large Scale Mapping. *Int. Arch. Photogramm. Remote Sens. Spatial Inf. Sci., XL-1/W4*, 47-54. <https://doi.org/10.5194/isprsarchives-XL-1-W4-47-2015>
- Mancini, F., Dubbini, M., Gattelli, M., Stecchi, F., Fabbri, S., Gabbianelli, G. (2013). Using Unmanned Aerial Vehicles (UAV) for High-Resolution Reconstruction of Topography: The Structure from Motion Approach on Coastal Environments. *Remote Sensing*, 5(12), 6880-6898.
- Michez, A., Philippe, L., David, K., Sébastien, C., Christian, D., Bindelle, J. (2020). Can Low-Cost Unmanned Aerial Systems Describe the Forage Quality Heterogeneity? Insight from a Timothy Pasture Case Study in Southern Belgium. *Remote Sensing*, 12(10), 1650.
- Moudrý, V., Urban, R., Štroner, M., Komárek, J., Brouček, J., Prošek, J. (2019). Comparison of a

- Commercial and Home-Assembled Fixed-Wing UAV for Terrain Mapping of a Post-Mining Site Under Leaf-Off Conditions. *International Journal of Remote Sensing*, 40(2), 555-572. <https://doi.org/10.1080/01431161.2018.1516311>
- Peng, Y., Tang, Z., Zhao, G., Cao, G., Wu, C. (2022). Motion Blur Removal for UAV-Based Wind Turbine Blade Images Using Synthetic Datasets. *Remote Sensing*, 14(1), 87.
- Pichaikuppan, V. R. A., Narayanan, R. A., Rangarajan, A. (2014). Change Detection in the Presence of Motion Blur and Rolling Shutter Effect. *Computer Vision – ECCV 2014*, Cham.
- Pricope, N. G., Mapes, K. L., Woodward, K. D., Olsen, S. F., Baxley, J. B. (2019). Multi-Sensor Assessment of the Effects of Varying Processing Parameters on UAS Product Accuracy and Quality. *Drones*, 3(3), 63.
- Rhee, S., Kim, T. (2016). Dense 3D Point Cloud Generation from UAV Images from Image Matching and Global Optimazation. *Int. Arch. Photogramm. Remote Sens. Spatial Inf. Sci.*, XLI-B1, 1005-1009. <https://doi.org/10.5194/isprs-archives-XLI-B1-1005-2016>
- Roth, L., Hund, A., Aasen, H. (2018). PhenoFly Planning Tool: Flight Planning for High-Resolution Optical Remote Sensing with Unmanned Aerial Systems. *Plant Methods*, 14(1), 116. <https://doi.org/10.1186/s13007-018-0376-6>
- Ruzgienė, B., Berteška, T., Gečyte, S., Jakubauskienė, E., Aksamitauskas, V. Č. (2015). The Surface Modelling Based on UAV Photogrammetry and Qualitative Estimation. *Measurement*, 73, 619-627. <https://doi.org/10.1016/j.measurement.2015.04.018>
- Santise, M., Fornari, M., Forlani, G., Roncella, R. (2014). Evaluation of DEM Generation Accuracy from UAS Imagery. *Int. Arch. Photogramm. Remote Sens. Spatial Inf. Sci.*, XL-5, 529-536. <https://doi.org/10.5194/isprsarchives-XL-5-529-2014>
- Sertić, H., Paar, R., Tomić, H., Ravlić, F. (2022). Influence of Flight Height and Image Sensor on the Quality of the UAS Orthophotos for Cadastral Survey Purposes. *Land*, 11(8), 1250.
- Shawky, M., Moussa, A., Hassan, Q. K., El-Sheimy, N. (2019). Pixel-Based Geometric Assessment of Channel Networks/Orders Derived from Global Spaceborne Digital Elevation Models. *Remote Sensing*, 11(3), 235.
- Sieberth, T., Wackrow, R., Chandler, J. H. (2014). Influence of blur on feature matching and a geometric approach for photogrammetric deblurring. *Int. Arch. Photogramm. Remote Sens. Spatial Inf. Sci.*, XL-3, 321-326. <https://doi.org/10.5194/isprsarchives-XL-3-321-2014>
- Sieberth, T., Wackrow, R., Chandler, J. H. (2015). UAV Image Blur and Its Influence and Ways to Correct It. *Int. Arch. Photogramm. Remote Sens. Spatial Inf. Sci.*, XL-1/W4, 33-39. <https://doi.org/10.5194/isprsarchives-XL-1-W4-33-2015>
- Teague, S., Chahl, J. (2023). Strapdown Celestial Attitude Estimation from Long Exposure Images for UAV Navigation. *Drones*, 7(1), 52.
- Uysal, M., Toprak, A. S., Polat, N. (2015). DEM Generation with UAV Photogrammetry and Accuracy Analysis in Sahitler Hill. *Measurement*, 73, 539-543. <https://doi.org/https://doi.org/10.1016/j.measurement.2015.06.010>
- Ventura, D., Bruno, M., Jona Lasinio, G., Belluscio, A., Ardizzone, G. (2016). A Low-Cost Drone Based Application for Identifying and Mapping of Coastal Fish Nursery Grounds. *Estuarine, Coastal and Shelf Science*, 171, 85-98. <https://doi.org/10.1016/j.ecss.2016.01.030>
- Villanueva, J. K. S., Blanco, A. C. (2019). Optimization of Ground Control Point (GCP) Configuration for Unmanned Aerial Vehicle (UAV) Survey Using Structure from Motion (SfM). *Int. Arch. Photogramm. Remote Sens. Spatial Inf. Sci.*, XLII-4/W12, 167-174. <https://doi.org/10.5194/isprs-archives-XLII-4-W12-167-2019>
- Wang, D., Shu, H. (2022). Accuracy Analysis of Three-Dimensional Modeling of a Multi-Level UAV without Control Points. *Buildings*, 12(5), 592.
- Wang, Y. Z., Ye, Q. H. (2021). ArcPycor: An Open-Source Automated GIS Tool to Co-Register Elevation Datasets. *Journal of Mountain Science*, 18(4), 923-931. <https://doi.org/10.1007/s11629-020-6305-y>
- Xu, N., Qin, R., Song, S. (2023). Point cloud registration for LiDAR and photogrammetric data: A critical synthesis and performance analysis on classic and deep learning algorithms. *ISPRS Open Journal of Photogrammetry and Remote Sensing*, 8, 100032. <https://doi.org/https://doi.org/10.1016/j.ophoto.2023.100032>
- Zapico, I., Laronne, J. B., Sánchez Castillo, L., Martín Duque, J. F. (2021). Improvement of Workflow for Topographic Surveys in Long Highwalls of Open Pit Mines with an Unmanned Aerial Vehicle and Structure from Motion. *Remote Sensing*, 13(17), 3353.
- Zhang, Z., Zhu, L. (2023). A Review on Unmanned Aerial Vehicle Remote Sensing: Platforms, Sensors, Data Processing Methods, and Applications. *Drones*, 7(6), 398.
- Zhou, Y., Daakir, M., Rupnik, E., Pierrot-Deseilligny, M. (2020). A Two-Step Approach for the Correction of Rolling Shutter Distortion in UAV Photogrammetry. *ISPRS Journal of Photogrammetry and Remote Sensing*, 160, 51-66. <https://doi.org/10.1016/j.isprsjprs.2019.11.020>